

Water Resources Research

RESEARCH LETTER

10.1029/2018WR024492

Key Points:

- The lower and upper part of the saltwater-freshwater interface are, respectively, affected by varying inland freshwater input and tides
- Interaction between tidal fluctuations and varying inland freshwater input is nonlinear
- Tide reduces the time lags in the response of the saltwater wedge and submarine groundwater discharge to the varying inland freshwater input

Correspondence to:

P. Xin,
pei.xin@outlook.com

Citation:

Kuan, W. K., Xin, P., Jin, G., Robinson, C. E., Gibbes, B., & Li, L. (2019). Combined effect of tides and varying inland groundwater input on flow and salinity distribution in unconfined coastal aquifers. *Water Resources Research*, 55, 8864–8880. <https://doi.org/10.1029/2018WR024492>

Received 1 JUL 2019

Accepted 2 OCT 2019

Accepted article online 26 OCT 2019

Published online 11 NOV 2019

Combined Effect of Tides and Varying Inland Groundwater Input on Flow and Salinity Distribution in Unconfined Coastal Aquifers

Woei Keong Kuan¹ , Pei Xin² , Guangqiu Jin² , Clare E. Robinson³ , Badin Gibbes⁴ , and Ling Li⁵ 

¹Faculty of Civil Engineering, Universiti Teknologi MARA, Cawangan Pulau Pinang, Permatang Pau, Malaysia, ²State Key Laboratory of Hydrology-Water Resources and Hydraulic Engineering, Hohai University, Nanjing, China,

³Department of Civil and Environmental Engineering, The University of Western Ontario, London, Ontario, Canada,

⁴School of Civil Engineering, The University of Queensland, Brisbane, Queensland, Australia, ⁵School of Engineering, Westlake University, Hangzhou, China

Abstract Tides and seasonally varying inland freshwater input, with different fluctuation periods, are important factors affecting flow and salt transport in coastal unconfined aquifers. These processes affect submarine groundwater discharge (SGD) and associated chemical transport to the sea. While the individual effects of these forcings have previously been studied, here we conducted physical experiments and numerical simulations to evaluate the interactions between varying inland freshwater input and tidal oscillations. Varying inland freshwater input was shown to induce significant water exchange across the aquifer-sea interface as the saltwater wedge shifted landward and seaward over the fluctuation cycle. Tidal oscillations led to seawater circulations through the intertidal zone that also enhanced the density-driven circulation, resulting in a significant increase in the total SGD. The combination of the tide and varying inland freshwater input, however, decreased the SGD components driven by the separate forcings (e.g., tides and density). Tides restricted the landward and seaward movement of the saltwater wedge in response to the varying inland freshwater input in addition to reducing the time delay between the varying freshwater input signal and landward-seaward movement in the saltwater wedge interface. This study revealed the nonlinear interaction between tidal fluctuations and varying inland freshwater input will help to improve our understanding of SGD, seawater intrusion, and chemical transport in coastal unconfined aquifers.

1. Introduction

In coastal aquifers, lateral hydraulic gradients towards the sea often exist. These hydraulic gradients drive inland fresh groundwater and land-sourced chemicals (e.g., nutrient, metal, and organic contaminant) to discharge to the sea. In the absence of dynamic oceanic forcing such as tides and waves, fresh groundwater flows above the saltwater wedge, resulting in a sloping freshwater-seawater mixing zone that starts around the intersection between the beach and mean sea level (Robinson et al., 2018). Due to diffusion, saline water in the saltwater wedge mixes with discharging fresh groundwater, resulting in a convective circulation through the saltwater wedge, that is, density-driven circulation (Cooper, 1959). The overall hydraulic gradients are controlled by the inland fresh groundwater input (or groundwater table) and mean sea level that determine the location of the saltwater wedge interface and the total efflux (both fresh groundwater and circulating seawater) to the sea. The total efflux to the sea is commonly termed submarine groundwater discharge (SGD). It has been widely identified, based on an assumption of equilibrium, that decreased inland fresh groundwater input leads to a landward shift in the saltwater wedge interface (seawater intrusion) and a decrease in the circulating seawater flux. On the contrary, increased fresh groundwater input shifts the saltwater wedge seaward, resulting in an increase in the density-driven circulation (Michael et al., 2005; Smith, 2004; Werner et al., 2013). In natural systems, inland fresh groundwater input varies seasonally in response to seasonal rainfall patterns and associated aquifer recharge (Charette, 2007; Loveless et al., 2008; Michael et al., 2005; Miyaoka, 2007; Moore, 2007; Sugimoto et al., 2016). This seasonal variation causes not only the saltwater wedge to oscillate landward and seaward but also the varying density-driven

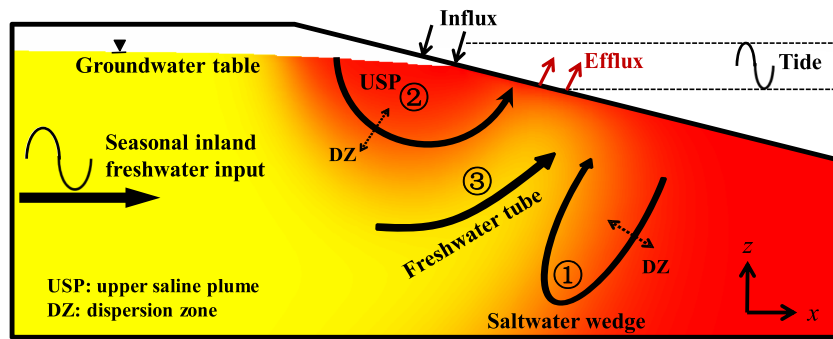


Figure 1. Schematic diagram of an unconfined aquifer including major flow processes considered in this study: (1) density-driven circulation, (2) tide-induced circulation, and (3) terrestrial groundwater discharge. The colors represent groundwater salinity (red for seawater and yellow for terrestrial fresh groundwater).

circulation to seasonal fluctuations in SGD (Michael et al., 2005). Furthermore, the response of both the saltwater wedge and SGD to varying seasonal inland fresh groundwater input are not instantaneous but delayed, resulting in time lags between the former two (saltwater wedge and SGD) and the latter (Michael et al., 2005).

Tides are an important oceanic force acting on coastal aquifers worldwide. In a tide-influenced aquifer, seawater infiltrates the upper intertidal zone during the rising tide and exfiltrates in the lower intertidal zone during the falling tide when the sea level drops below the local groundwater table. This often leads to a phase-averaged seawater circulation in the intertidal zone and a salinity distribution often referred to as an upper saline plume (USP). As such, fresh groundwater discharges in a freshwater tube between the USP and the saltwater wedge (Figure 1; Abarca et al., 2013; Boufadel, 2000; Buquet et al., 2016; Dale & Miller, 2007; Heiss & Michael, 2014; Kuan et al., 2012; Robinson, Gibbes, et al., 2007; Robinson et al., 2006; Vandenbohede & Lebbe, 2007). Tide-induced circulation across the aquifer-sea interface has been shown to contribute greatly to the total SGD (Li et al., 1999; Moore et al., 2008; Robinson, Li, & Barry, 2007; Robinson et al., 2018; Yu et al., 2019) and influences the transport pathway and fate of land-sourced chemicals in the aquifer prior to discharge to the ocean (Anwar et al., 2014; Burnett et al., 2003; Charette & Buesseler, 2004; Heiss et al., 2017; Heiss & Michael, 2014; Moore, 1999; Robinson et al., 2009; Santos et al., 2008; Santos et al., 2014; Simmons, 1992). Furthermore, tides also affect the location of the lower saltwater wedge interface and thickness of the saltwater-freshwater mixing zone. It has been suggested that the presence of tides can inhibit seawater intrusion, lead to a thicker mixing zone, and subsequently modify the density-driven circulation and total SGD (Kuan et al., 2012; Robinson, Li, & Barry, 2007; Xin et al., 2015).

Early studies of SGD widely assumed that the total SGD is a simple and linear sum of the SGD components caused by individual forcing factors (Burnett et al., 2006; Li et al., 1999; Taniguchi et al., 2002). For instance, considering the inland fresh groundwater input, density-driven circulation, and tidal influence,

$$\text{SGD} = \text{FSGD} + Q_D + Q_T, \quad (1)$$

where FSGD is the fresh SGD at the seaside, Q_D is the density-driven circulation, and Q_T is the tide-induced circulation. Fresh SGD is expected to be delayed and vary seasonally in response to seasonal fluctuations in inland freshwater input.

Recent studies have challenged this linear model (equation (1)), suggesting that interactions among the different forcing factors are likely nonlinear (King, 2012; Xin et al., 2015). For example, Robinson, Li, and Barry (2007) and Robinson, Li, and Prommer (2007) showed that tides can increase the density-driven circulation and saline SGD. Xin et al. (2010) suggested that the combined influence of tides and waves is less than the saline SGDs induced by these two forces separately. Considering time scales, the response of SGD and salinity distribution to the different forces is not instantaneous but delayed (Heiss & Michael, 2014; Liu et al., 2016; Lu & Werner, 2013; Michael et al., 2005; Robinson et al., 2014; Xin et al., 2014). As such, in understanding the functioning of a coastal aquifer we need to consider the present as well as the past nonlinear interactions among different forces acting on the system (Xin et al., 2014; Xin et al., 2015).

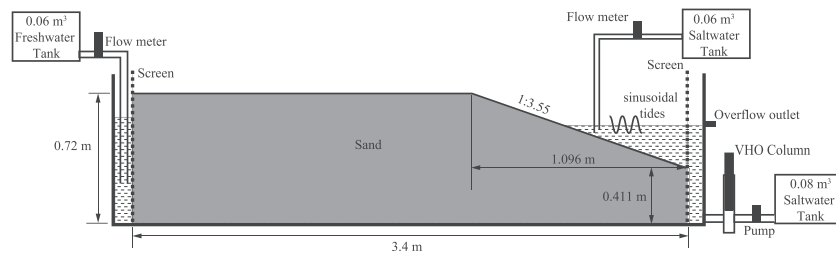


Figure 2. Schematic diagram of the laboratory experiment setup (a) and numerical model (b) including the boundary conditions adopted (modified after Kuan et al., 2012). VHO = variable height overflow.

While the importance of nonlinear interactions between the different forces acting on coastal aquifers has been clearly illustrated, few studies have explored these interactions (see details in review in Robinson et al., 2018). Particularly, the combined effect of tides and varying inland groundwater input on flow and salt transport in coastal unconfined aquifers is poorly understood. Most analytical, experimental, and numerical studies on seawater intrusion neglect the effects of dynamic oceanic forcing (Werner et al., 2013). On the other hand, research examining the effects of oceanic forcing on SGD and seawater intrusion generally consider only a fixed inland freshwater input or groundwater table (Robinson et al., 2018; Werner et al., 2013). Recently, Liu et al. (2016) showed that the USP expanded and contracted and the saltwater-freshwater interface oscillated landward and seaward in response to a fluctuating inland groundwater level. The magnitude of tide-induced seawater circulation was found to vary based on the fluctuating inland groundwater level. Yu et al. (2017) demonstrated that long- and short-term variations in SGD from a coastal aquifer subject to irregular inland freshwater input were strongly affected by the interactions with oceanic forcing. While these two numerical studies demonstrate the importance of combined inland freshwater conditions and tides in controlling the SGD and salt transport in a coastal aquifer, it remains unclear how the tides and varying inland freshwater input, with different fluctuation periods, interact in unconfined coastal aquifers.

In this study, we conducted laboratory experiments and numerical simulations to investigate the behavior of the saltwater wedge and water exchange across the aquifer-ocean interface under the combined influence of tidal fluctuations and varying inland groundwater input. The purpose of the study was to address the following key questions. (1) How does the tide affect the oscillation of the saltwater-freshwater interface over the cycle of varying inland groundwater input? (2) How do the tidal fluctuations and varying inland freshwater input interact to affect SGD? (3) How does the tide modify the temporal response (time lags) of the saltwater-freshwater interface and SGD to varying inland groundwater input? Answers to these questions are needed to better understand the interplay of oceanic and terrestrial forces in controlling saltwater intrusion and SGD.

2. Methodology

2.1. Laboratory Experiments

Experiments were conducted in a sand flume with dimensions of 3.5-m length, 0.8-m height, and 0.02-m width. The sand flume was divided into three compartments: a freshwater reservoir at the landward boundary, a saltwater reservoir at the seaward boundary, and a middle compartment packed with quartz sand (Figure 2). This experimental setup, similar to Kuan et al. (2012), is essentially a 2-D unconfined aquifer with a beach slope of 1:3.55, allowing examination of the flow and salt transport processes in a laboratory-scale unconfined coastal aquifer in the vertical and cross-shore direction.

Prior to the experiment, the sand was washed with deionized water and packed carefully to avoid air-trapping in the sand flume. The grain size distribution of the sand was relatively uniform with the median diameter $d_{50} = 0.24$ mm and $d_{90}/d_{10} = 2.86$ (d_{90} and d_{10} are, respectively, the sieve size that 90% and 10% of sand grains pass through). The average saturated hydraulic conductivity value measured for the packed porous medium was 5.26×10^{-3} m/s using an in situ method based on steady flows. The porosity of the sand was measured to be 0.46 using the imbibition method (Collins, 1961).

Table 1
Experiment Setup and Key Results of Calculated Recirculation Rates Across the Aquifer-Ocean Interface per Unit Width of Aquifer^a

Boundary condition			Circulation rate (m ³ /day/m)					Circulation percentage (%);		
Case Number	Case name	Tide	Inland freshwater input (m ³ /day/m)	Freshwater discharge	Tide induced	Density driven	Total submarine groundwater discharge	Freshwater discharge	Tide induced	Density driven
1	No Tide-Q(0.720)	Without	0.720	0.720	0.000	0.065	0.785	92	0	8
2	No Tide-Q(1.728)	Without	1.728	1.728	0.000	0.079	1.807	96	0	4
3	No Tide-Q(2.592)	Without	2.592	2.592	0.000	0.086	2.678	97	0	3
4	Tide-Q(0.720)	With	0.720	0.720	1.908	1.310	3.938	18	48	33
5	Tide-Q(1.728)	With	1.728	1.728	1.598	1.469	4.795	36	33	31
6	Tide-Q(2.592)	With	2.592	2.592	0.986	1.570	5.148	50	19	30
7	No Tide-SE	Without	Varying	1.728	0.000	0.137	1.865	93	0	7
8	Tide-SE	With	Varying	1.728	1.339	1.584	4.651	37	29	34

^aAveraged over a seasonal cycle of the inland freshwater input (720 min).

A steady state flow was established through the flume with a constant flow of 1.728 m³/day/m (per unit meter width flux) deionized water into the freshwater reservoir. The inland freshwater flux was controlled using a variable area flow meter. Under the nontidal condition, saltwater was supplied from a 0.06-m³ saltwater tank at a preset rate greater than the freshwater discharge rate to maintain a relatively constant salinity in the near-shore zone. An overflow outlet maintained the water level in the near-shore zone at mean sea level, which was set at 0.55 m above the tank bottom (Figure 2). For the experiments with tidal fluctuations, saltwater flowed in and out of the saltwater reservoir and near-shore zone through a variable height overflow column designed to simulate simple sinusoidal tides acting on the beach surface (Cartwright et al., 2003). A tidal amplitude (A_T) of 0.043 m and tidal period (T) of 62 s were applied for all tidal cases (Table 1). Both the salinity and water level in the near-shore zone were monitored throughout the experiments.

The experiments were conducted under fixed and varying inland freshwater input conditions with and without tides. A total of eight experiments were run until the flow and salt distribution reached a steady state under the nontidal condition or quasi steady (periodic) state under the tidal condition (Table 1). Under the fixed inland freshwater input condition, the inland freshwater input rates were set as 0.720, 1.728, and 2.592 m³/day/m (details in Table 1).

All experiments were started by simulating a fixed inland freshwater input without the influence of tides (Cases 1–3, Table 1). This was then followed by including the tidal condition with the same fixed inland freshwater input (Cases 4–6, Table 1). The experiments considering varying inland freshwater input were started after the steady/quasi steady state (nontidal/tidal case) was achieved (Cases 7–8, Table 1). To simulate the varying flux condition, the inland freshwater input was varied every 30 min over a period of 12 hr. As such, the seasonal period was equivalent to 697 tidal cycles (this period ratio is close to that in a natural system with seasonal variations in freshwater input and a semidiurnal tide [365×2]). The experiments were continued for five seasonal cycles (60 hr) for both the tidal and nontidal cases. The average inland freshwater influx for these cases was 1.728 m³/day/m with a standard variation of 0.525 m³/day/m (Table 1).

The saltwater solution was prepared by dissolving 33.4 g of sodium chloride and 1.6 g of red food dye in a liter of deionized water. The density of the saltwater was measured at 1.026 g/ml in the saltwater tank and maintained throughout the experiments. The result of sorption tests, following the method of Goswami and Clement (2007) showed that there was no sorption of dye by the porous medium. High-resolution digital photographs were taken at a fixed interval to track the salinity distribution in the sand flume (Chang & Clement, 2012, 2013; Goswami & Clement, 2007; Kuan et al., 2012). The color photographs were converted to gray scale images, which were further processed in a binary fashion (black and white image) by automatically calculating the optimum threshold values using Otsu's method (Otsu, 1979) to minimize the intraclass variance of the continuous images. These black-white images enabled consistent delineation of the interface between the fresh (white) and saline (black) water in the aquifer.

2.2. Numerical Modeling

A numerical model, SUTRA (Voss & Provost, 2002) was used to further investigate the interaction between tides and terrestrial forces in controlling the oscillations of the saltwater-freshwater interface and flux across the aquifer-sea interface. In SUTRA, variably-saturated, variable-density flow is governed by the Richards equation, and this is coupled with the advection-diffusion equation for solute transport (Voss & Provost, 2002). The numerical model was first tested to evaluate the consistency of the simulated results with the laboratory data and afterwards extended to a field-scale unconfined aquifer system to further investigate the phenomena observed at the laboratory scale.

The laboratory-scale numerical model was set up to simulate the laboratory experimental conditions (Figure 2). The seaward boundary section below the sea surface was set as a specified-pressure boundary subjected to the hydrostatic pressure corresponding to the seawater depth. The section above the sea surface was specified according to the following two conditions: (1) if the (exposed) nodes were saturated at the previous time step, they were taken as part of a seepage face with pressure equal to zero (atmospheric pressure); and (2) if the nodes were unsaturated at the previous time step, they were treated as a no-flow boundary (Xin et al., 2010). For salt transport, the seawater concentration was set to be 35 ppt (mass fraction, parts per thousand) for (seawater) inflow to the aquifer, and zero concentration gradient was specified for outflow from the aquifer.

The van Genuchten (1980) functions were adopted to specify the relationship between the hydraulic conductivity, soil saturation, and capillary pressure head in the numerical model. Typical values of the soil water retention parameters for sand (Carsel & Parrish, 1988) were applied in the functions. The residual water saturation of sand was set to 0.1 while the van Genuchten (1980) soil water retention parameters a and n were set to 5.9 and 2.68 m^{-1} , respectively. The diffusivity (D_f), longitudinal (α_L), and transversal (α_T) dispersivity coefficients, respectively, of $1 \times 10^{-9} \text{ m}^2/\text{s}$, 0.002 m, and 0.0004 m were used following the study of Kuan et al. (2012).

An adaptive mesh refinement strategy was used to optimize the computational performance. The domain of the laboratory-scale model was divided into a rectangular inland sub-domain, a sloping intertidal sub-domain, and a rectangular seabed sub-domain. The mesh was refined increasingly from the inland to the seaward boundary in the sloping intertidal sub-domain where the USP formed. Tests were conducted to ensure that the numerical solutions were converged and independent of the time step and mesh size. All simulations were run until the numerical solutions had reached the quasi steady state with respect to both hydraulic heads and salt concentrations under fixed inland input conditions.

To generalize the finding, we also conducted simulations on a field-scale unconfined aquifer. The field-scale numerical model was set up based on a shallow unconfined aquifer on Moreton Island, Australia, following the study of Xin et al. (2010). A 2-D vertical cross-shore slice of the coastal aquifer was simulated with a length of 200 m and depth of 33 m. Following Xin et al. (2010), the aquifer was assumed to be homogeneous and isotropic with hydraulic conductivity of 10 m/d, soil porosity of 0.45, longitudinal dispersivity of 0.5 m, and transverse dispersivity of 0.05 m (see further details in Xin et al., 2010). The simulated inland groundwater input varied seasonally (sinusoidal cycle) with oscillation amplitude of $1.05 \text{ m}^3/\text{day}/\text{m}$ for a period of 360 days. Based on Xin et al. (2010), the mean Q_{in} was $2.1 \text{ m}^3/\text{day}/\text{m}$ per unit width. Two field-scale simulation cases were considered: without and with tide. For the latter, a semidiurnal tide with amplitude of 1 m and period of 0.5 days was simulated.

3. Results

In this section, the results for the steady state and quasi steady state experiments with fixed inland freshwater input are first presented (section 3.1). As salt distributions under similar forcing conditions have been described previously (Robinson et al., 2018; Werner et al., 2013), we focus our discussion on the interactions between the different forcings. Following this, we analyze the time-varying salt distribution and flux across the aquifer-sea interface for experiments with both inland freshwater input and tides (sections 3.2 and 3.3). Finally, we use the numerical model to upscale the findings by simulating the flow and salt transport processes in a field-scale unconfined aquifer (section 3.4).

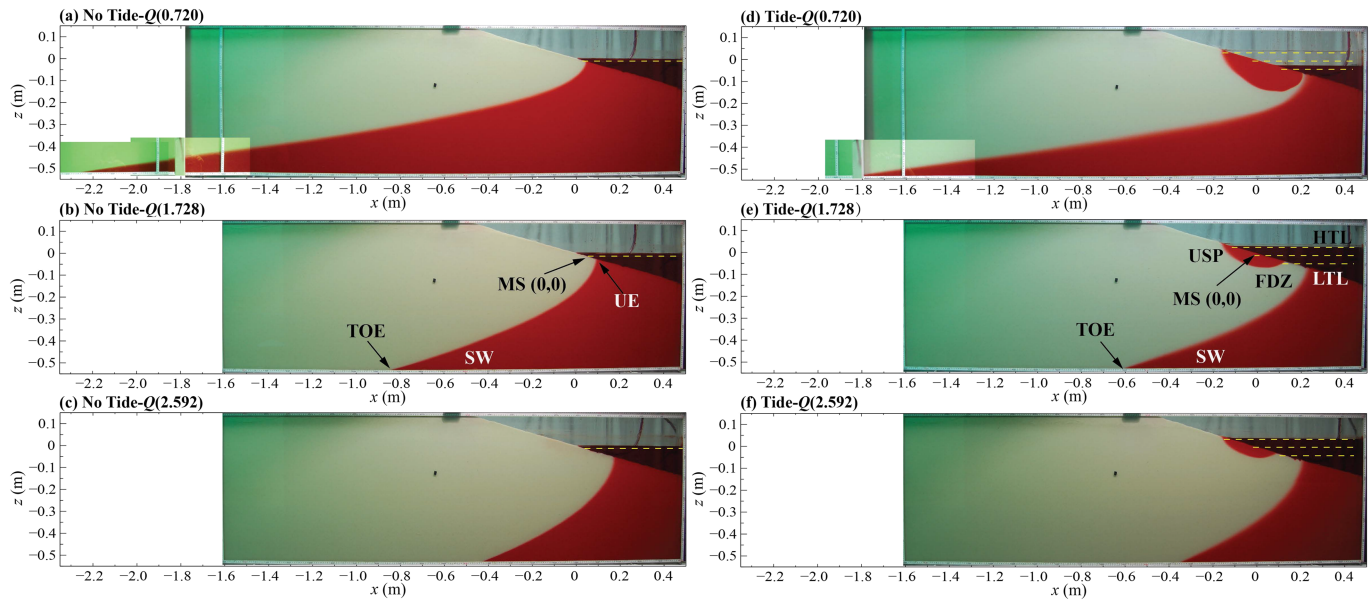


Figure 3. Images of the salt distribution in the sand flume for the laboratory-scale study cases at the quasi steady state under the fixed freshwater input condition. The lower saltwater wedge (SW), toe of the saltwater wedge (TOE), upper edge of saltwater wedge (UE), upper saline plume (USP), freshwater discharge zone (FDZ), mean shoreline (MS), high tide level (HTL) and low tide level (LTL) are indicated.

3.1. Salinity Distributions and Circulation Rate at the Quasi Steady States

For the nontidal cases, as expected the saltwater wedge retreated seaward as the inland freshwater input increased. As Q_{in} increased from 0.720 to 1.728, and 2.592 m³/day/m, the toe location moved from −2.24 to −0.83 and −0.42 m, respectively (Figures 3a–3c). This was consistent with previous studies (Goswami & Clement, 2007; Kuan et al., 2012). With the tidal cases, an USP formed in the shallow aquifer (Figures 3d–3f). In comparison with the nontidal cases, the tide pushed the saltwater wedge seaward. With respect to the saltwater wedge movement, the interaction between the tide and inland freshwater input was nonlinear. The tides damped the movement of the saltwater wedge in response to the changing inland freshwater input. For example, the toe location only moved from −1.81 to −0.60 and −0.34 m as Q_{in} increased from 0.720 to 1.728, and 2.592 m³/day/m, respectively. On the other hand, the changing inland freshwater input also altered the influence of the tide on the salinity distribution. As Q_{in} increased, the USP contracted in both depth and horizontal extension. As such, the zone of freshwater between the USP and saltwater wedge expanded. This is clearly seen in Figure 3 whereby the two saline water cells almost merged up for the experiment with $Q_{in} = 0.720$ m³/day/m (Figure 3d), but with $Q_{in} = 2.592$ m³/day/m, the horizontal width of the freshwater discharge zone (0.12 m) was similar to the horizontal extent of the USP (0.17 m; Figure 3f).

Using the numerical model, we were able to calculate the fluxes across the aquifer-sea interface that were not possible to measure during the laboratory experiments (Table 1, note that we have validated the model against the salinity distribution from the lab experiments and the results were consistent). For the nontidal cases, the density-driven circulation flux increased from 0.065 to 0.079, and 0.086 m³/day/m as Q_{in} increased from 0.720 to 1.728, and 2.592 m³/day/m. While both the density-driven circulation and Q_{in} increased, the increase rate in the former was less than that in the latter. As such, the contribution of density-driven circulation to the total SGD decreased, that is, it decreased from 8% to 4% to 3% as Q_{in} increased from 0.720 to 1.728, and 2.592 m³/day/m.

As shown in prior studies, consideration of tidal fluctuations modified the groundwater flow patterns and the water exchange across the aquifer-sea interface. For example, with Q_{in} fixed at 0.720 m³/day/m, the tide-induced circulation flux was 1.908 m³/day/m (2.65 times Q_{in}), and the density-driven circulation flux increased from 0.065 (without tide) to 1.310 m³/day/m (increased by around 19-fold). With tides considered, tide-induced and density-driven circulation dominated the total SGD (48% and 33%, respectively; Table 1).

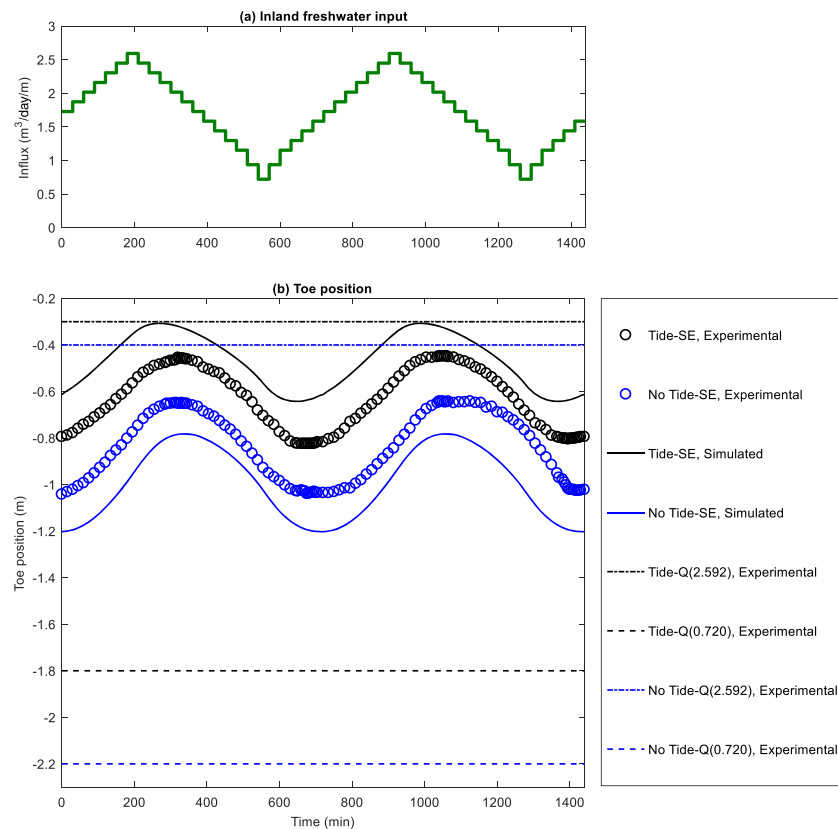


Figure 4. (a) Seasonal fluctuating inland freshwater input. (b) Experimental and numerical simulation results of the saltwater wedge toe positions (note that the elapsed days were referred to the beginning of the fourth inland freshwater cycle). For comparison, the saltwater wedge toe positions with the fixed freshwater input are also given (horizontal lines).

As Q_{in} increased from 0.720 to 1.728, and 2.592 $\text{m}^3/\text{day}/\text{m}$, the tide-induced circulation flux decreased from 1.908 to 1.598, and 0.986 $\text{m}^3/\text{day}/\text{m}$, respectively. This interaction between the forcings is nonlinear. For instance, an increase of 140% in Q_{in} (from 0.720 to 1.728 $\text{m}^3/\text{day}/\text{m}$) resulted in 16% reduction in the tide-induced circulation. An increase of 260% in Q_{in} (from 0.720 to 2.592 $\text{m}^3/\text{day}/\text{m}$) resulted in 48% reduction in the tide-induced circulation. These nonlinear change rates suggested that the inhibition of inland freshwater input on the tide-induced circulation was accelerated. For constant tidal condition, an increase in Q_{in} increased the density-driven flux—this was similar to the cases without the tide. However, the rates at which the density-driven flux increased as the Q_{in} increased were different between the cases without and with tides considered. As Q_{in} increased from 0.720 to 1.728 and to 2.592 $\text{m}^3/\text{day}/\text{m}$, the density-driven circulation flux increased by 12% and 20%, respectively (relative to that for $Q_{in} = 0.720 \text{ m}^3/\text{day}/\text{m}$), for cases with the tide. These relative increases in the density-driven circulation were overall less than those for the cases without the tide where the density-driven circulation increased by 22% and 32%, respectively.

Based on the conditions examined here, an increase in Q_{in} enhanced the density-driven circulation but reduced the tide-induced circulation. Overall, the total SGD increased. Quantifying the total increase in SGD, the percentage increase in SGD was lower than the percentage increase in Q_{in} . As Q_{in} increased from 0.720 to 1.728, and 2.592 $\text{m}^3/\text{day}/\text{m}$, the total SGD increased from 3.938 to 4.795 $\text{m}^3/\text{day}/\text{m}$ (by 1.2 times; less than 1.4 times for Q_{in}) and 5.148 $\text{m}^3/\text{day}/\text{m}$ (by 1.7 times; less than 2.6 times for Q_{in}). These results suggest that in unconfined coastal aquifers, the interaction between density-driven and tide-induced circulations and inland freshwater input is complex and nonlinear.

3.2. Variation of Salinity Distributions Caused by Varying Inland Freshwater Input

With the inland freshwater input varying periodically (Figure 4a), the overall horizontal hydraulic gradient changed, resulting in changes in the salinity distribution. For both the experimental cases without and with

tides, the location of the saltwater wedge toe shifted seaward and landward as Q_{in} increased and decreased, respectively (Figure 4). However, this response was not instantaneous but delayed relative to the variations in Q_{in} . The digital photographs failed to delineate a freshwater-seawater mixing zone, but rather a sharp interface. The observed time delays in the cases without and with tide differed slightly, in contrast to the apparent difference from the simulation results. While the initial peak in Q_{in} occurred at Minute 180, the corresponding times at which the location of the saltwater wedge toe was the most seaward were Minutes 305 and 296 (average over five seasonal cycle) for the cases with and without tides, respectively. This delay (~120 min) was around 1/6 of the fluctuation cycle of Q_{in} . We also quantified the movement of the 50% isohaline of the seawater based on the numerical simulation results (note that the simulated toe movement differed from that of the experiments where only a sharp saltwater-freshwater interface could be tracked. The discrepancy is explained further below). For the case without tides, the simulated time at which the saltwater wedge toe was the most seaward occurred at Minute 330. This was a larger lag time compared with the corresponding experiment. For the case with tides, the simulated time at which the saltwater wedge toe was the most seaward occurred at Minute 270. This was a smaller lag time compared with the corresponding experiment. Based on the simulation results, the tide decreased the time delay by 60 min.

Based on the experimental results, the Q_{in} variations overall led to a freshwater-saltwater interface closer to the inland boundary for the nontidal case (Figure 5), compared to the tidal cases (Figure 6). For the former, the location of the saltwater wedge toe moved between -1.05 and -0.63 m, while for the latter, it moved between -0.82 and -0.44 m in response to the fluctuations in Q_{in} . It is interesting that the movement range in the saltwater wedge toe was similar for both cases (0.42 m compared to 0.38 m), suggesting that the movement of the toe was controlled by the inland freshwater input regardless of the mean position of the toe (-0.84 m vs. -0.63 m). We also compared the center positions of the toe fluctuation with those with fixed Q_{in} . In contrast, they (for Q_{in} varying between 0.720 and 2.592 m³/day/m) were close to that with Q_{in} fixed at 2.592 m³/day/m and much farther from that with Q_{in} fixed at 0.720 m³/day/m (Figure 4b). For example, the toe under the varying Q_{in} fluctuated around -0.63 m in the tidal case, being close to -0.34 m with Q_{in} fixed at 2.592 m³/day/m. This further highlights the nonlinear response of the location of the saltwater wedge toe to the periodic variations in Q_{in} . The asymmetric response of the saltwater wedge movement (intrusion and retreat) to the inland freshwater table variations was consistent with previous studies (Abdoulhalik & Ahmed, 2018; Chang & Clement, 2012; Morgan et al., 2013). As the inland freshwater flow was in the same direction of seawater retreat, the effect of the varying Q_{in} contributed unequally to seawater intrusion and seawater retreat, which draws the overall saltwater wedge toe seaward (close to the one induced by a fixed and larger Q_{in}).

It is well established that dynamic variations at either the inland or seaward boundaries of a coastal aquifer enhance freshwater-saltwater mixing and increase the thickness of the mixing zone (Robinson et al., 2018; Werner et al., 2013). Here we examined the combined effect of both inland and seaward fluctuations in the lab-scale aquifer. For the experimental results, movement in the sharp freshwater-saltwater interface over the Q_{in} cycle as detected using color images is shown in Figures 7a and 7b. For the simulation results, we averaged the salinity distribution over a Q_{in} cycle (Figures 7c and 7d). Similar to previous laboratory experiments (Abdoulhalik & Ahmed, 2018; Kuan et al., 2012; Morgan et al., 2013), it was only possible to delineate a sharp freshwater-saltwater interface using the dye-tracking method, and the width of the mixing zone could not be quantified. As such, the locations of the saltwater wedge toe as indicated by the simulated 50% isohaline differed from the toe locations determined via the laboratory experiments (Figure 4b). Nevertheless, both the laboratory and numerical simulation results demonstrated the enhanced mixing due to the combined Q_{in} and tidal fluctuations. Without the tide, the Q_{in} variations led to a thick mixing zone, around 0.4 m in thickness at the bottom of the aquifer (Figures 7a and 7c). The tide pushed the mixing zone seaward, and its modification on the mixing was in twofold. For the lower saltwater wedge, the tidal effect appeared insignificant with the thickness of the mixing zone only changing slightly (Figure 7a compared with Figure 7b, and Figure 7c compared with Figure 7d). In the shallow aquifer near the aquifer-sea interface, for the nontidal case, movement in the freshwater-saltwater interface in response to the varying Q_{in} was small due to the fixed sea level (Figures 7a and 7c). In the tidal case, this dynamic seaward boundary led to the formation of a USP and a considerably thicker mixing zone associated with the saltwater wedge (Figure 7c compared with Figure 7d). Furthermore, the USP and width of the

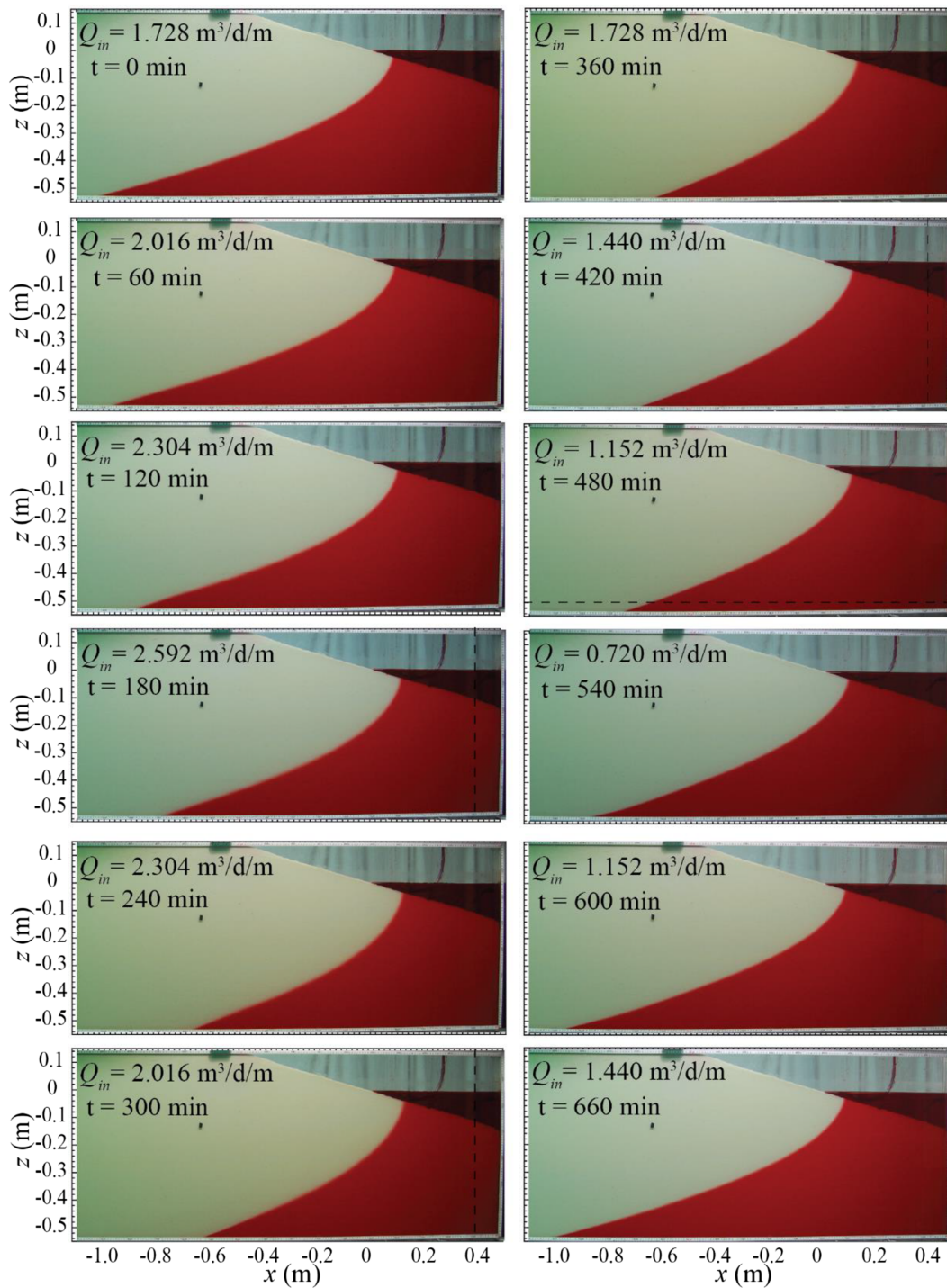


Figure 5. Images of saltwater wedge movement at 60-min interval under nontidal conditions (No Tide-SE) over one 12-hr seasonal cycle (fourth seasonal cycle) for the laboratory-scale study cases.

freshwater discharge zone both expanded and contracted in response to the varying Q_{in} (Figure 6). Overall the results revealed that while the tide and fluctuating Q_{in} interacted in the aquifer, their combined effect on mixing depended on the distance to the forcing boundaries. For instance, tidal modification was concentrated in the shallow aquifer near the aquifer-sea interface where the tide most affected the groundwater flow patterns. This was consistent with the well-known theory of groundwater propagation in unconfined aquifers.

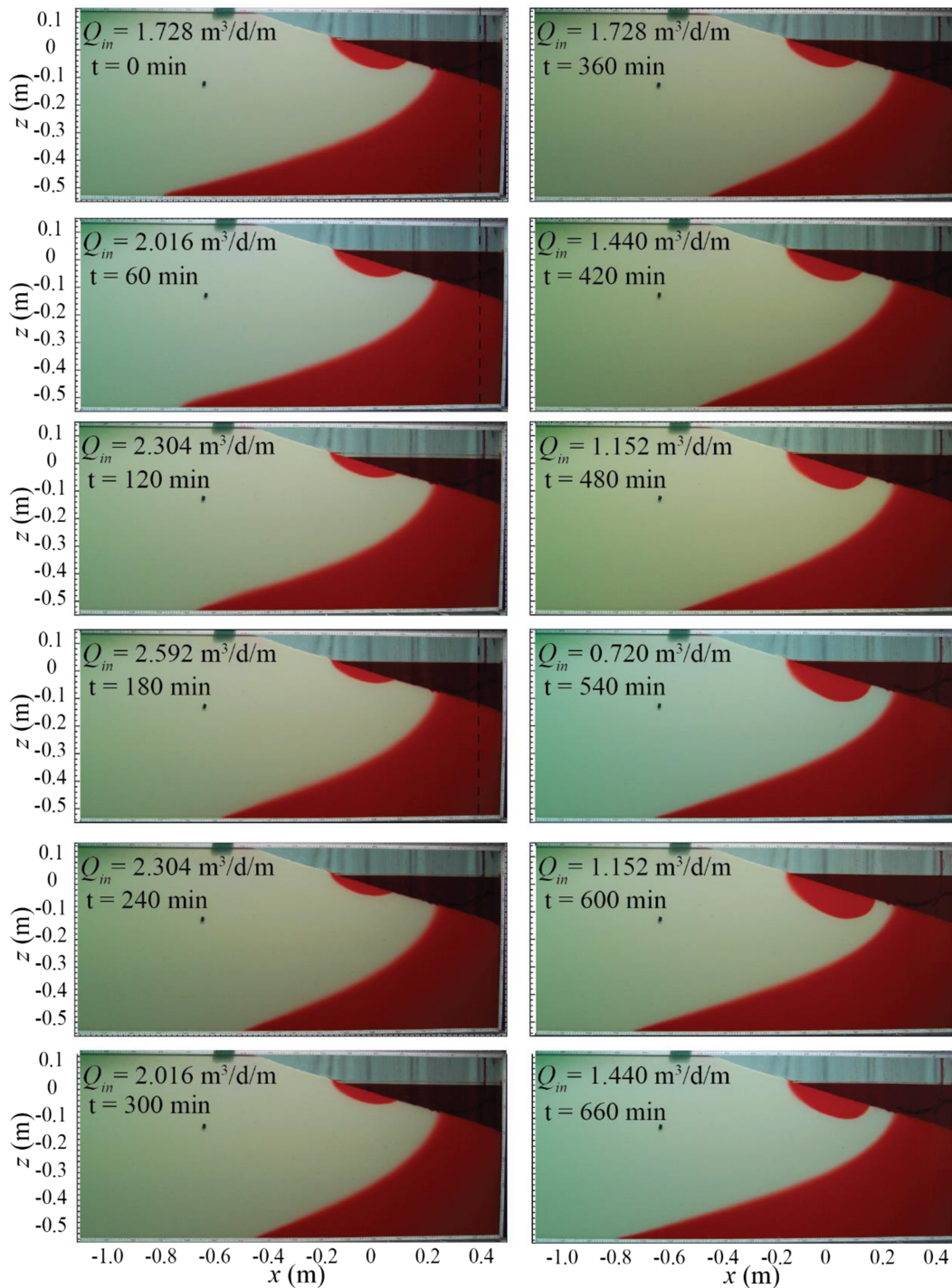


Figure 6. Images of saltwater wedge movement at 60-min interval under tidal conditions (Tide-SE) over one 12-hr seasonal cycle (fourth seasonal cycle) for the laboratory-scale study cases.

3.3. Variation of Fluxes Across the Aquifer-Sea Interface Caused by Varying Inland Freshwater Input

The fluxes across the aquifer-sea interface were calculated using the numerical simulation results. Specifically, the tide-induced water influx (Figure 8a), density-driven water influx (Figure 8b), total water efflux (SGD, Figure 8c), and freshwater efflux (freshwater SGD) were calculated. Treating salt as a tracer, we determined the freshwater SGD as follows (Figures 8d and 8e):

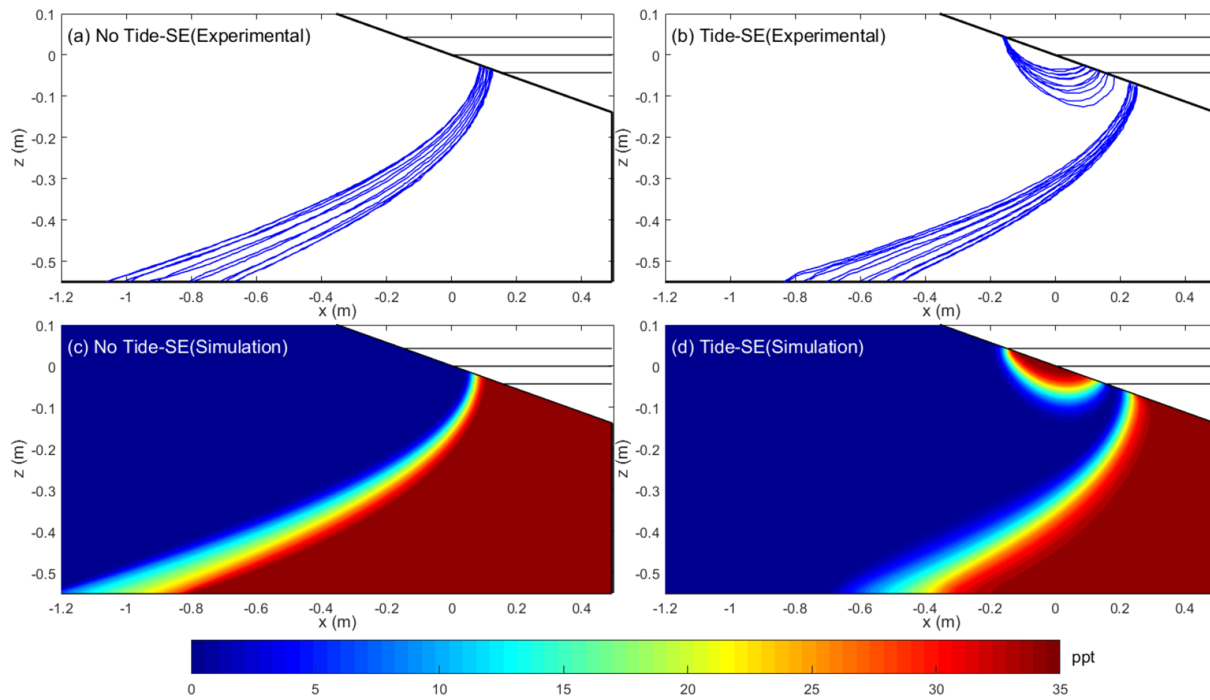


Figure 7. Experimental and numerical simulation results of the range of saltwater-freshwater interface oscillations over a seasonal cycle with no tide (a and c) and with tide (b and d). For the experiments, the interface was delineated by using black-white images (a for the images in Figure 5 and b for the images in Figure 6); while as for the numerical simulations, (b and d) show the salinity distribution averaged over a seasonal cycle of inland freshwater input (12 hr).

$$\text{freshwater SGD} = \text{total water efflux} - \frac{\text{total salt efflux}}{\text{seawater salinity}}. \quad (2)$$

As expected, the tide-induced influx decreased as Q_{in} increased. This was consistent with the changes in the size of the shallow tide-induced seawater circulations and USP as Q_{in} varied (Figure 8a). However, the variation of tide-induced influx was slightly asymmetric relative to changes in Q_{in} . The period for the increasing tide-induced influx took 386 min (from Minute 184 to Minute 570, Figure 8a), which was 54% of the period of the Q_{in} fluctuation (i.e., 12 hr). This led to an averaged tide-induced influx of $1.339 \text{ m}^3/\text{day}/\text{m}$ which was slightly smaller than the mean value ($1.447 \text{ m}^3/\text{day}/\text{m}$) with Q_{in} fixed at 0.720 and $2.592 \text{ m}^3/\text{day}/\text{m}$ (Table 1).

For the nontidal case, the density-driven influx was negligible when Q_{in} was large (e.g., from Minute 0 to Minute 300, Figure 8a) due to the large overall horizontal hydraulic gradient and water flow towards the sea (Figure 8d). Density-driven influx only occurred during 55% of the Q_{in} cycle (between Minute 300 to Minute 698) with the flux increasing as Q_{in} decreased. This was significantly altered by the tide with density-driven influx occurring throughout the Q_{in} cycle for the tidal case. Furthermore, it was relatively constant around $1.584 \text{ m}^3/\text{day}/\text{m}$ and much larger than for the nontidal case (varying between 0 and $0.47 \text{ m}^3/\text{day}/\text{m}$). The larger density-driven influx for the tidal case was likely due to enhanced hydrodynamic dispersion across the saltwater wedge dispersion zone caused by tidal fluctuations.

The total efflux (SGD) followed the variation in Q_{in} although with a small time lag (around 13 min). The temporal trends for the cases without and with tides were similar while the total SGD magnitude for the nontidal case was much less than for the tidal case ($1.865 \text{ m}^3/\text{d}/\text{m}$ vs. $4.651 \text{ m}^3/\text{day}/\text{m}$). The total time-varying influx to the coastal aquifer (summation of Q_{in} , tide-induced influx and density-driven influx) was similar to the time-varying total efflux with the total influx and efflux nearly synchronous for the laboratory-scale aquifer (Figure 8c). This suggested that the total SGD across the aquifer-sea interface was almost a simple linear sum of the SGD components caused by the different forcing. Nevertheless, the different forcing interacted together such that the influxes across the aquifer-sea interface were considerably different from the influxes driven by the individual forcing alone.

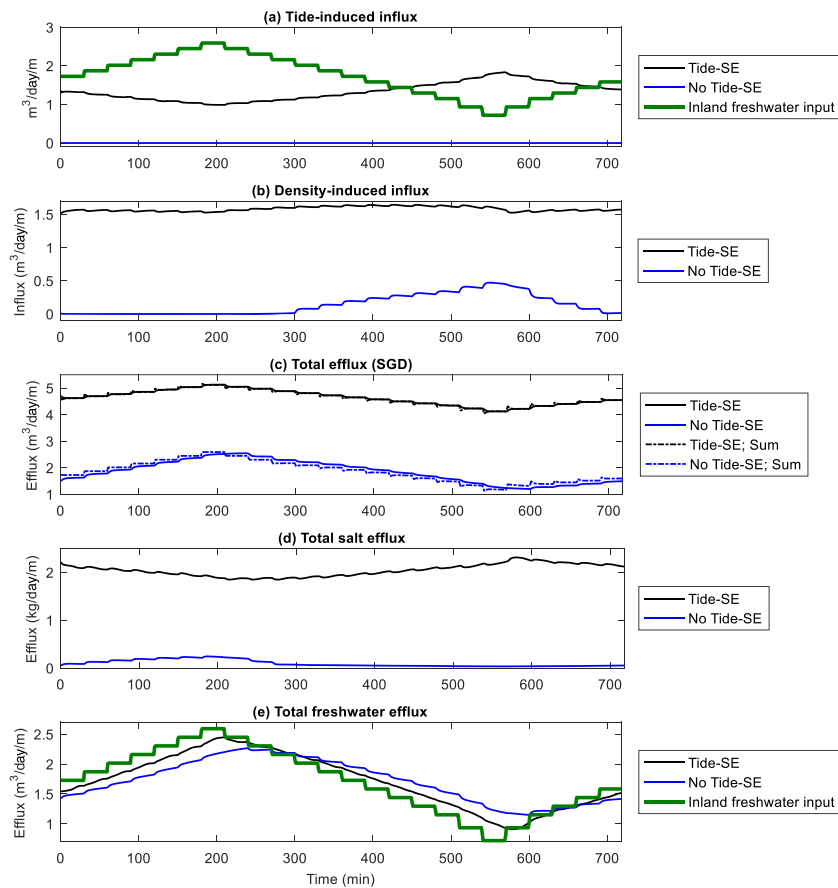


Figure 8. Fluxes across the aquifer-sea interface: (a) tide-induced water influx, (b) density-driven water influx, (c) total water efflux (SGD), (d) total salt efflux, and (e) total freshwater efflux. In (a) and (e), variation of inland freshwater input was also demonstrated. In (c), the summation of the time-dependent inland freshwater input, tide-induced influx, and density-driven influx was also shown in comparison with the calculated total water efflux. SGD = submarine groundwater discharge.

Due to the time for the fresh groundwater to be transported through the coastal aquifer, the fluctuations in freshwater SGD was delayed relative to the Q_{in} fluctuations (Figure 8e). In the case without tide, the delay was approximately 57 min (8% of the Q_{in} cycle). This delay was significantly reduced for the tidal case to 21 min (3% of the Q_{in} cycle). For the nontidal case, the variations in the freshwater SGD to the sea were moderated only by variations in the density-driven circulations. However, for the tidal case, the changing tide-induced circulations and associated expansion and contraction of the USP changed the width of the freshwater discharge zone which the narrowing of this zone reduces the delay in the freshwater SGD relative to the Q_{in} variations.

3.4. Results From Field-Scale Numerical Simulations

Overall, the results from the field-scale simulations were consistent with those at laboratory-scale indicating that the phenomena observed at the laboratory-scale also occur at the field scale (Figure 9). The saltwater wedge toe shifted in response to the seasonally varying Q_{in} with the movement delayed relative to the Q_{in} fluctuations. The tide decreased the time delay in comparison with the nontidal case (20% of the the period of the Q_{in} fluctuation in comparison with 26% for the nontidal case). Furthermore, the tide restricted the landward and seaward movement in the saltwater wedge toe, that is, toe moved between -13.9 and -7.9 m (range = 6.0 m) for the tidal case compared to that between -43.6 and -35.3 m (range = 8.3 m) for the nontidal case.

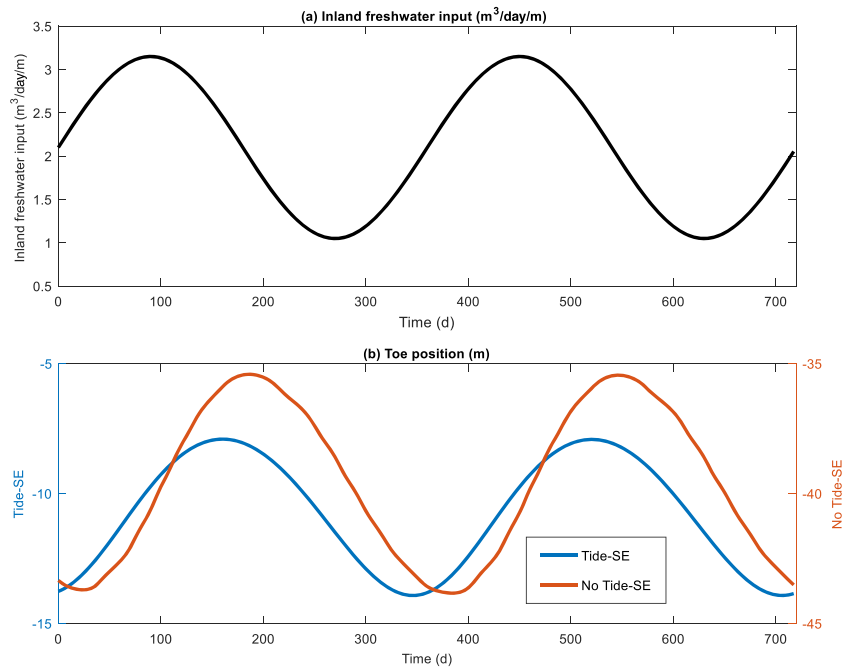


Figure 9. (a) Seasonal fluctuating inland freshwater input. (b) Simulated saltwater wedge toe position in the field-scale aquifer.

Tidal fluctuations induced significant seawater circulations across the aquifer-sea interface (Figure 10a) and also increased the density-driven circulations (Figure 10b). The increase in these circulations led the total SGD to increase more than twofold ($5.1 \text{ m}^3/\text{day}/\text{m}$ for the tidal case compared with $2.5 \text{ m}^3/\text{day}/\text{m}$ for the

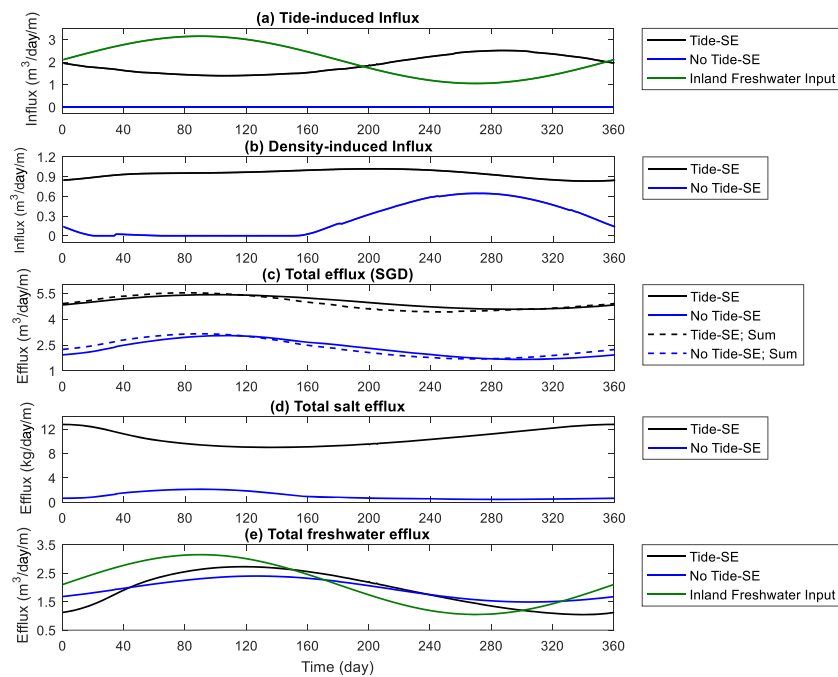


Figure 10. (a) Fluxes across the aquifer-sea interface: (a) tide-induced water influx, (b) density-driven water influx, (c) total water efflux (SGD), (d) total salt efflux and (e) total freshwater efflux. In (a) and (e), variation of inland freshwater input was also demonstrated. In (c), the summation of the time-dependent inland freshwater input, tide-induced influx and density-driven influx was also shown in comparison with the calculated total water efflux. SGD = submarine groundwater discharge.

nontidal case; Figure 10c). In contrast to that at the laboratory-scale, the total time-varying influx to the coastal aquifer (summation of Q_{in} , tide-induced influx and density-driven influx) differed slightly from the time-varying total efflux (Figure 10c), resulting in varying water storage in the aquifer (i.e., based on the mass conservation principle). As such, the varying total SGD across the aquifer-sea interface was no longer consistent with the simple linear sum of the time-dependent SGD components caused by the different forcings.

Similar to the laboratory experiments, fluctuations in the freshwater SGD were delayed and damped relative to the Q_{in} variations (Figures 10d and 10e). Consistent with the movement of the saltwater wedge toe, the tide was found to damp the amplitude of the freshwater SGD fluctuations as well as reduce the time delay relative to the nontidal case, for example, the time delay was reduced from 8% to 26% of the seasonal cycle for the tidal case compared to the nontidal case.

4. Discussion

Freshwater input to coastal aquifers is variable over time due to changes in the natural recharge patterns as well as anthropogenic groundwater extraction and recharge. Varying inland freshwater input alters the extent of seawater intrusion into a coastal aquifer and thus affects the availability of fresh groundwater resources. Assessment of seawater intrusion and groundwater resources at regional scales tend to focus on the impact of varying inland freshwater input and neglect the effects of dynamic oceanic forcing (Robinson et al., 2018; Werner et al., 2013). Our results indicate that tidal fluctuations may push the interface of the saltwater wedge seaward and thus increase the freshwater storage in the aquifer. As such it is important to consider the effect of tides on the movement of the saltwater wedge in addition to the effects of varying inland freshwater input along tidally dominated coastlines as tides may considerably alter freshwater storage in the coastal aquifer at spatiotemporal scales.

Our results show that at the laboratory scale, the total SGD across the aquifer-sea interface was almost a simple linear sum of the SGD components caused by the different forcing (Burnett et al., 2006; Li et al., 1999; Taniguchi et al., 2002), that is, the total combined SGD was similar to the sum of the density-driven influx, tide-induced influx, and inland freshwater input. This may have been because the laboratory-scale aquifer adjusted rapidly to changing forcing conditions such that the influxes and effluxes across the boundary balanced each other. However, the different forcings interacted together such that the influxes across the aquifer-sea interface differed considerably from the influxes driven by the individual forcing alone. For example, the density-driven influx for the tidal case was 1.5 times higher than for the nontidal case. This non-linear interaction between the forcings may need to be considered when separating the various SGD components for real field systems.

Driven by lateral hydraulic gradients, inland fresh groundwater and land-sourced chemicals are transported to the sea. Distinguishing the inland fresh groundwater flux from the total SGD is often needed to calculate the flux of land-derived chemicals to the sea. However, this remains a challenge as typically the isotope methods used to determine SGD volumes in the field are only about to determine the total SGD. Our simulation results showed fluctuations in the freshwater SGD are not synchronous with the inland freshwater input, with the freshwater SGD significantly delayed relative to fluctuations in the inland freshwater inputs to the coastal aquifer. This has important implications in assessment of the temporal trends in chemical fluxes to the sea as it cannot be assumed that the highest freshwater SGD and thus land-derived chemical flux occurs when the inland water table is highest.

The ability to predict the magnitude as well as the timing of chemicals fluxes to the ocean is important for understanding the impact of SGD on nearshore water quality and ecosystems. For instance, higher SGD nitrogen loads in summer months may exacerbate nearshore eutrophic conditions associated with the warmer temperatures (Gonneea & Charette, 2014). The time delay we observed between the inland freshwater variations and fresh SGD flux at the seaside needs to be considered in predicting the timing of land-derived chemicals to the ocean with our experiments indicating that this time delay is reduced along tidally dominated coasts. It is well established that the saltwater-freshwater mixing zones associated with the saltwater wedge and USP are hotspots of biogeochemical reactivity with groundwater-seawater mixing dynamics playing a key role in controlling chemical fluxes to the sea (Anwar et al., 2014; Gonneea & Charette, 2014; Heiss et al., 2017; Robinson et al., 2009). Our results show that the interplay between the tides and variations in the

freshwater input further complicate the mixing conditions in the aquifer. While tides lead to the formation of a USP and thereby enhance mixing in the shallow intertidal aquifer, tides were found to restrict the seasonal landward-seaward shift of the saltwater wedge interface in the shallow aquifer. Understanding the movement of this interface is important because it affects the fate and temporal fluxes of dissolved trace metals and nutrients that are sensitive to changes in ionic strength and redox conditions (Gonneea et al., 2013; Gonneea & Charette, 2014).

5. Conclusions

This study examined the combined influence of tides and varying inland groundwater input on the behavior of the saltwater wedge and water exchange across the aquifer-sea interface. Based on the experimental and simulation results the key new findings from the study are the following:

1. Fluctuations of inland freshwater input led the saltwater-freshwater interface to oscillate landward and seaward in coastal aquifers without and with tides. The landward-seaward movement in the saltwater wedge interface was greater in the deeper aquifer compared with that near the aquifer-sea boundary. The tide pushed the overall saltwater-freshwater interface seaward and led to the formation of an USP in the shallow aquifer. The upper part of the lower saltwater wedge varied following tidal fluctuation, resulting in enhanced mixing.
2. The tide enhanced significantly the seasonal aquifer-sea water exchange under the varying inland freshwater input not only by causing shallow circulation but also by enhancing the density-driven circulation. In this way, the total SGD increased remarkably (by 150% in comparison with the case without tide at the laboratory-scale). The interactions among inland groundwater input, tide-induced, and density-driven fluxes were nonlinear.
3. The response of the salinity distribution in the coastal aquifer and the fluxes across the aquifer-sea interface were delayed relative to the variations in the inland groundwater input. The time delay was decreased by the presence of tidal fluctuations.

It is worth noting that this study assumed the coastal aquifer was homogeneous and isotropic and also uniform in the alongshore direction. In reality, coastal aquifers are often heterogeneous, and anisotropy and beach morphology vary in the alongshore direction. Furthermore, only semidiurnal tides were considered. Oceanic forcing including waves and multiple constituent tidal signals may lead to more complex flow and solute transport dynamics. Further studies are required to include hydrogeological and morphological complexities and additional oceanic forces. In this study, the dye-tracking method delineated a sharp saltwater-freshwater interface during the experiment. It is desirable to quantify the saltwater-freshwater mixing in physical laboratory and field systems using ideal solutions. Nevertheless, the results presented here provide important insights on the nonlinear interaction between coastal aquifers and sea, which are needed to better understand and predict salt and chemical transport in coastal unconfined aquifers.

Acknowledgments

This work was supported by the National Natural Science Foundation of China (51579077). The authors acknowledge valuable comments from the managing editor (Jean Bahr), the associate editor, and three anonymous reviewers, which led to significant improvement of the paper. The used numerical model, SUTRA, can be downloaded from the USGS website (<https://www.usgs.gov/software/sutra-a-model-2d-or-3d-saturated-unsaturated-variable-density-ground-water-flow-solute-or>). The experimental data and numerical simulation results in this study are available in the CHUAHSI Hydroshare database (<http://www.hydroshare.org/resource/b06b0db7c05842559fab94abd8c6a5da>).

References

- Abarca, E., Karam, H., Hemond, H. F., & Harvey, C. F. (2013). Transient groundwater dynamics in a coastal aquifer: The effects of tides, the lunar cycle, and the beach profile. *Water Resources Research*, 49, 2473–2488. <https://doi.org/10.1002/wrcr.20075>
- Abdoulhalik, A., & Ahmed, A. A. (2018). Transience of seawater intrusion and retreat in response to incremental water-level variations. *Hydrological Processes*, 32(17), 2721–2733. <https://doi.org/10.1002/hyp.13214>
- Anwar, N., Robinson, C., & Barry, D. A. (2014). Influence of tides and waves on the fate of nutrients in a nearshore aquifer: Numerical simulations. *Advances in Water Resources*, 73, 203–213. <https://doi.org/10.1016/j.advwatres.2014.08.015>
- Boufadel, M. C. (2000). A mechanistic study of nonlinear solute transport in a groundwater-surface water system under steady state and transient hydraulic conditions. *Water Resources Research*, 36(9), 2549–2565. <https://doi.org/10.1029/2000WR900159>
- Buquet, D., Sirieix, C., Anschutz, P., Malaurent, P., Charbonnier, C., Naessens, F., et al. (2016). Shape of the shallow aquifer at the fresh water-sea water interface on a high-energy sandy beach. *Estuarine, Coastal and Shelf Science*, 179, 79–89. <https://doi.org/10.1016/j.ecss.2015.08.019>
- Burnett, W. C., Aggarwal, P. K., Aureli, A., Bokuniewicz, H., Cable, J. E., Charette, M. A., et al. (2006). Quantifying submarine groundwater discharge in the coastal zone via multiple methods. *Science of the Total Environment*, 367(2–3), 498–543. <https://doi.org/10.1016/j.scitotenv.2006.05.009>
- Burnett, W. C., Bokuniewicz, H., Huettel, M., Moore, W. S., & Taniguchi, M. (2003). Groundwater and pore water inputs to the coastal zone. *Biogeochemistry*, 66(1/2), 3–33. <https://doi.org/10.1023/B:BIOG.0000006066.21240.53>
- Carsel, R. F., & Parrish, R. S. (1988). Developing joint probability distributions of soil water retention characteristics. *Water Resources Research*, 24(5), 755–769. <https://doi.org/10.1029/WR024i005p00755>
- Cartwright, N., Nielsen, P., & Dunn, S. (2003). Water table waves in an unconfined aquifer: Experiments and modeling. *Water Resources Research*, 39(12), 1330. <https://doi.org/10.1029/2003wr002185>

- Chang, S. W., & Clement, T. P. (2012). Experimental and numerical investigation of saltwater intrusion dynamics in flux-controlled groundwater systems. *Water Resources Research*, 48, W09527. <https://doi.org/10.1029/2012WR012134>
- Chang, S. W., & Clement, T. P. (2013). Laboratory and numerical investigation of transport processes occurring above and within a salt-water wedge. *Journal of Contaminant Hydrology*, 147, 14–24. <https://doi.org/10.1016/j.jconhyd.2013.02.005>
- Charette, M. A. (2007). Hydrologic forcing of submarine groundwater discharge: Insight from a seasonal study of radium isotopes in a groundwater-dominated salt marsh estuary. *Limnology and Oceanography*, 52(1), 230–239. <https://doi.org/10.4319/lo.2007.52.1.0230>
- Charette, M. A., & Buesseler, K. O. (2004). Submarine groundwater discharge of nutrients and copper to an urban subestuary of Chesapeake Bay (Elizabeth River). *Limnology and Oceanography*, 49(2), 376–385. <https://doi.org/10.4319/lo.2004.49.2.0376>
- Collins, R. E. (1961). *Flow of fluids through porous materials*. New York: Reinhold Pub. Corp.
- Cooper, H. H. (1959). A hypothesis concerning the dynamic balance of fresh water and salt water in a coastal aquifer. *Journal of Geophysical Research*, 64(4), 461–467. <https://doi.org/10.1029/JZ064i004p00461>
- Dale, R. K., & Miller, D. C. (2007). Spatial and temporal patterns of salinity and temperature at an intertidal groundwater seep. *Estuarine, Coastal and Shelf Science*, 72(1–2), 283–298. <https://doi.org/10.1016/j.ecss.2006.10.024>
- Gonneea, M. E., & Charette, M. A. (2014). Hydrologic controls on nutrient cycling in an unconfined coastal aquifer. *Environmental Science & Technology*, 48, 14,178–14,185. <https://doi.org/10.1021/es503313t>
- Gonneea, M. E., Mulligan, A. E., & Charette, M. A. (2013). Climate-driven sea level anomalies modulate coastal groundwater dynamics and discharge. *Geophysical Research Letters*, 40, 2701–2706. <https://doi.org/10.1002/grl.50192>
- Goswami, R. R., & Clement, T. P. (2007). Laboratory-scale investigation of saltwater intrusion dynamics. *Water Resources Research*, 43, W04418. <https://doi.org/10.1029/2006wr0005151>
- Heiss, J. W., & Michael, H. A. (2014). Saltwater-freshwater mixing dynamics in a sandy beach aquifer over tidal, spring-neap, and seasonal cycles. *Water Resources Research*, 50, 6747–6766. <https://doi.org/10.1002/2014WR015574>
- Heiss, J. W., Post, V. E. A., Laattoe, T., Russoniello, C. J., & Michael, H. A. (2017). Physical controls on biogeochemical processes in intertidal zones of beach aquifers. *Water Resources Research*, 53, 9225–9244. <https://doi.org/10.1002/2017WR021110>
- King, J. N. (2012). Synthesis of benthic flux components in the Patos Lagoon coastal zone, Rio Grande do Sul, Brazil. *Water Resources Research*, 48, W12530. <https://doi.org/10.1029/2011wr011477>
- Kuan, W. K., Jin, G., Xin, P., Robinson, C., Gibbes, B., & Li, L. (2012). Tidal influence on seawater intrusion in unconfined coastal aquifers. *Water Resources Research*, 48, W02502. <https://doi.org/10.1029/2011wr010678>
- Li, L., Barry, D. A., Stagnitti, F., & Parlange, J.-Y. (1999). Submarine groundwater discharge and associated chemical input to a coastal sea. *Water Resources Research*, 35(11), 3253–3259. <https://doi.org/10.1029/1999WR900189>
- Liu, Y., Jiao, J. J., & Luo, X. (2016). Effects of inland water level oscillation on groundwater dynamics and land-sourced solute transport in a coastal aquifer. *Coastal Engineering*, 114, 347–360. <https://doi.org/10.1016/j.coastaleng.2016.04.021>
- Loveless, A. M., Oldham, C. E., & Hancock, G. J. (2008). Radium isotopes reveal seasonal groundwater inputs to Cockburn Sound, a marine embayment in Western Australia. *Journal of Hydrology*, 351(1), 203–217. <https://doi.org/10.1016/j.jhydrol.2007.12.010>
- Lu, C., & Werner, A. D. (2013). Timescales of seawater intrusion and retreat. *Advances in Water Resources*, 59, 39–51. <https://doi.org/10.1016/j.advwatres.2013.05.005>
- Michael, H. A., Mulligan, A. E., & Harvey, C. F. (2005). Seasonal oscillations in water exchange between aquifers and the coastal ocean. *Nature*, 436(7054), 1145–1148. <https://doi.org/10.1038/nature03935>
- Miyaoka, K. (2007). Seasonal changes in the groundwater-seawater interaction and its relation to submarine groundwater discharge, Ise Bay, Japan. Paper presented at the IAHS-AISH Publication.
- Moore, W. S. (1999). The subterranean estuary: A reaction zone of ground water and sea water. *Marine Chemistry*, 65(1–2), 111–125. [https://doi.org/10.1016/S0304-4203\(99\)00014-6](https://doi.org/10.1016/S0304-4203(99)00014-6)
- Moore, W. S. (2007). Seasonal changes in the radium-226 distribution on the southeastern USA continental shelf: Implications for changing submarine groundwater discharge. Paper presented at the IAHS-AISH Publication.
- Moore, W. S., Sarmiento, J. L., & Key, R. M. (2008). Submarine groundwater discharge revealed by Ra-228 distribution in the upper Atlantic Ocean. *Nature Geoscience*, 1(5), 309–311. <https://doi.org/10.1038/ngeo183>
- Morgan, L. K., Stoeckl, L., Werner, A. D., & Post, V. E. A. (2013). An assessment of seawater intrusion overshoot using physical and numerical modeling. *Water Resources Research*, 49, 6522–6526. <https://doi.org/10.1002/wrcr.20526>
- Otsu, N. (1979). A threshold selection method from gray-level histogram. *IEEE Transactions on Systems, Man, and Cybernetics*, 9(1), 62–66. <https://doi.org/10.1109/TSMC.1979.4310076>
- Robinson, C., Brovelli, A., Barry, D. A., & Li, L. (2009). Tidal influence on BTEX biodegradation in sandy coastal aquifers. *Advances in Water Resources*, 32(1), 16–28. <https://doi.org/10.1016/j.advwatres.2008.09.008>
- Robinson, C., Gibbes, B., Carey, H., & Li, L. (2007). Salt-freshwater dynamics in a subterranean estuary over a spring-neap tidal cycle. *Journal of Geophysical Research*, 112, C09007. <https://doi.org/10.1029/2006jc003888>
- Robinson, C., Gibbes, B., & Li, L. (2006). Driving mechanisms for groundwater flow and salt transport in a subterranean estuary. *Geophysical Research Letters*, 33, L03402. <https://doi.org/10.1029/2005gl025247>
- Robinson, C., Li, L., & Barry, D. A. (2007). Effect of tidal forcing on a subterranean estuary. *Advances in Water Resources*, 30(4), 851–865. <https://doi.org/10.1016/j.advwatres.2006.07.006>
- Robinson, C., Li, L., & Prommer, H. (2007). Tide-induced recirculation across the aquifer-ocean interface. *Water Resources Research*, 43, W07428. <https://doi.org/10.1029/2006wr005679>
- Robinson, C., Xin, P., Li, L., & Barry, D. A. (2014). Groundwater flow and salt transport in a subterranean estuary driven by intensified wave conditions. *Water Resources Research*, 50, 165–181. <https://doi.org/10.1002/2013WR013813>
- Robinson, C. E., Xin, P., Santos, I. R., Charette, M. A., Li, L., & Barry, D. A. (2018). Groundwater dynamics in subterranean estuaries of coastal unconfined aquifers: Controls on submarine groundwater discharge and chemical inputs to the ocean. *Advances in Water Resources*, 115, 315–331. <https://doi.org/10.1016/j.advwatres.2017.10.041>
- Santos, I. R., Bryan, K. R., Pilditch, C. A., & Tait, D. R. (2014). Influence of porewater exchange on nutrient dynamics in two New Zealand estuarine intertidal flats. *Marine Chemistry*, 167, 57–70. <https://doi.org/10.1016/j.marchem.2014.04.006>
- Santos, I. R., Burnett, W. C., Chanton, J., Mwashote, B., Suryaputra, I. G. N. A., & Dittmar, T. (2008). Nutrient biogeochemistry in a Gulf of Mexico subterranean estuary and groundwater-derived fluxes to the coastal ocean. *Limnology and Oceanography*, 53(2), 705–718. <https://doi.org/10.4319/lo.2008.53.2.0705>
- Simmons, G. M. (1992). Importance of submarine Groundwater discharge (SGWD) and seawater cycling to material flux across sediment water interfaces in marine environments. *Marine Ecology Progress Series*, 84(2), 173–184. <https://doi.org/10.3354/meps084173>

- Smith, A. J. (2004). Mixed convection and density-dependent seawater circulation in coastal aquifers. *Water Resources Research*, 40, W08309. <https://doi.org/10.1029/2003wr002977>
- Sugimoto, R., Honda, H., Kobayashi, S., Takao, Y., Tahara, D., Tominaga, O., & Taniguchi, M. (2016). Seasonal changes in submarine groundwater discharge and associated nutrient transport into a tideless semi-enclosed embayment (Obama Bay, Japan). *Estuaries and Coasts*, 39(1), 13–26. <https://doi.org/10.1007/s12237-015-9986-7>
- Taniguchi, M., Burnett, W. C., Cable, J. E., & Turner, J. V. (2002). Investigation of submarine groundwater discharge. *Hydrological Processes*, 16(11), 2115–2129. <https://doi.org/10.1002/hyp.1145>
- van Genuchten, M. T. (1980). A closed-form equation for predicting the hydraulic conductivity of unsaturated soils. *Soil Science Society of America Journal*, 44(5), 892–898. <https://doi.org/10.2136/sssaj1980.03615995004400050002x>
- Vandenbohede, A., & Lebbe, L. (2007). Effects of tides on a sloping shore: Groundwater dynamics and propagation of the tidal wave. *Hydrogeology Journal*, 15(4), 645–658. <https://doi.org/10.1007/s10040-006-0128-y>
- Voss, C. I., & Provost, A. M. (2002). *SUTRA, A model for saturated-unsaturated variable-density ground-water flow with solute or energy transport* (Vol. 2). Reston, Virginia: U.S. Geological Survey.
- Werner, A. D., Bakker, M., Post, V. E. A., Vandenbohede, A., Lu, C., Ataie-Ashtiani, B., et al. (2013). Seawater intrusion processes, investigation and management: Recent advances and future challenges. *Advances in Water Resources*, 51, 3–26. <https://doi.org/10.1016/j.advwatres.2012.03.004>
- Xin, P., Robinson, C., Li, L., Barry, D. A., & Bakhtyar, R. (2010). Effects of wave forcing on a subterranean estuary. *Water Resources Research*, 46, W12505. <https://doi.org/10.1029/2010wr009632>
- Xin, P., Wang, S. S. J., Lu, C., Robinson, C., & Li, L. (2015). Nonlinear interactions of waves and tides in a subterranean estuary. *Geophysical Research Letters*, 42, 2277–2284. <https://doi.org/10.1002/2015GL063643>
- Xin, P., Wang, S. S. J., Robinson, C., Li, L., Wang, Y., & Barry, D. A. (2014). Memory of past random wave conditions in submarine groundwater discharge. *Geophysical Research Letters*, 41, 2401–2410. <https://doi.org/10.1002/2014GL059617>
- Yu, X., Xin, P., Lu, C., Robinson, C., Li, L., & Barry, D. A. (2017). Effects of episodic rainfall on a subterranean estuary. *Water Resources Research*, 53, 5774–5787. <https://doi.org/10.1002/2017WR020809>
- Yu, X., Xin, P., Wang, S. S. J., Shen, C., & Li, L. (2019). Effects of multi-constituent tides on a subterranean estuary. *Advances in Water Resources*, 124, 53–67. <https://doi.org/10.1016/j.advwatres.2018.12.006>